Proceedings of the 1966 Linear Accelerator Conference, Los Alamos, New Mexico, USA

BEAM LOADING EFFECTS IN STANDING WAVE LINACS

T. Nishikawa
Department of Physics
University of Tokyo
Bunkyoku, Tokyo, Japan

1. Introduction

Current development of linear accelerators has made it possible to accelerate a beam current of more than hundred milliampares at high energies. In such a high current linac, the power absorbed in the beam is comparable to the power dissipated in walls. Accordingly beam effects on the accelerating field become appreciable.

Beam loading in electron linacs of the traveling-wave type has been studied by Saxon, Neal, Leiss et al.[1] During the last few years, ion sources have been improved to provide the same order of magnitudes of proton currents as electron's. Now, a number of laboratories are considering to construct high current proton linacs. In contrast to electron linacs, particle velocities in proton linacs will still be changing in the energy range of interest, so that the proper control of accelerating field under the presense of beam loading is of great importance. From this reason, the standing-wave type is usually adopted for the acceleration of protons.[2] In the traveling-wave case the correct distribution of the axial accelerating field can be set up only for a particular value of beam current, while, in the standing-wave type, it may be reproduced for any beam currents by changing the input power. In order to find proper design of standing-wave linacs, however, some features of beam effects different from those in traveling wave linacs must carefully be examined.

Beam effects in standing-wave linacs can be treated in the same line as in the traveling-wave type by superposing two waves in opposite directions. Lapostolle has developed a theory in this line with a dielectric waveguide model.[3] We have developed another method based on the microwave cavity theory, i. e. the normal mode analysis of standing-wave linacs.[4] In this paper a brief review of beam effects in standing-wave linacs will be described in terms of the latter method. An equivalent circuit analogy, such as presented by Nagle, Knapp, and others,[5] will also give most of the aspects discussed below.

2. Principle of Normal Mode Analysis

From microwave cavity theory, it is always possible to expand the actual field in terms of the normal modes which form an orthogonal set of functions obtained from the field in an ideal cavity. If such a normal mode of the linac cavity is well defined and sufficiently separated from its nearby modes, then normal mode analysis will be a useful method to examine the various effects caused by any perturbations or interactions inside the cavity. Taking the normal electric field, $\vec{E}_n(z, r, \theta)$, one can express the actual field as

$$\vec{E}(z,r,\theta,t) = \sum_n V_n(t)\,\vec{E}_n(z,r,\theta). \quad (1)$$

From Maxwell's equations and orthogonal relations, the expansion coefficient of $V_n(t)$ satisfies the equation of forced oscillation,[6]

$$\frac{d^2V_n}{dt^2} + \omega_n^2 V_n = -\frac{\omega_n}{\sqrt{\varepsilon\mu}}\int_S (\vec{E}\times\vec{H}_n)\cdot\vec{n}\,ds + \frac{1}{\varepsilon}\frac{d}{dt}\int_{S'} (\vec{H}\times\vec{E}_n)\cdot\vec{n}\,ds - \frac{1}{\varepsilon}\frac{d}{dt}\int \vec{J}\cdot\vec{E}_n\,dv. \quad (2)$$

The first term on the right hand side is integrated over the non-ideal conducting surfaces, S, such as lossy metallic walls of the cavity. By means of the standard evaluation of Q_0 from wall losses, this can be rewritten as a damping term,

$$-(1+j)\frac{\omega_n}{Q_0}\frac{dV_n}{dt}. \quad (3)$$

The surface integral in the second term is performed over the non-ideal open surface, S', and gives the effect of coupling the cavity to an outside system. One part of this term gives forced oscillation by an external souce and the other additional damping due to circuit losses ($\propto 1/Q_{ext}$). Effects of the beam within the cavity are obtained from the last term where the current density $\vec{J}$ at a point is multiplied by the normal electric field at that point and intergrated over the cavity volume. Assuming simple expressions for normal mode fields, a well-padded generator coupled to the cavity through S', and a constant uniform bunched beam along the cavity axis, one can solve the equation (2) for examples of the existing or the proposed standing-wave linacs. The detailed analysis has already been reported in reference 4. Some results and their comparisons with experiments will be given in the followings.

3. Excitation of Drift-tube Cavity

First consider excitation of a drift-tube cavity without beam. Because of wall losses, excitation of the field in a linac cavity along its long length is not simple. If one consider a TM_{010} normal mode field of a cylindrical cavity, one faces the fact that there is no Poynting vector along the length. On the other hand, for an actual cavity, the power flow through a cross section which compensates at least wall losses is always needed. In terms of normal mode analysis, this can be achieved due to the hybridization of nearby modes with the dominant mode. Together with the tangential magnetic field of the dominant mode, tangential components of the electric field in TM_{01n} modes ($n \neq 0$) are responsible for the composition of the energy flow.

If we assume that $V_n(t)$ in Eq. (1) varies as $\exp(j\omega_0' t)$, we obtain from Eqs. (2) and (3) that

$$V_n(t) \propto \left[\omega_n^2 - \omega_0'^2 - (1-j)\,\frac{\omega_0'\,\omega_n}{Q_0}\right]^{-1}. \qquad (4)$$

Thus, if the mode separation is large compared to the width of resonances, nearby mode fields will be about 90° out of phase with the dominant mode for which the reasonance condition, $\omega_0' \approx \omega_0(1-1/2Q_0)$, is satisfied. Including the axial variation of the normal mode field, the amplitude of a nearby mode in a steady state can be written thus,

$$2\,\eta_n\,E_0\,\frac{\omega_0^2}{Q_0}\,\frac{\cos n\pi z/L}{\omega_n^2 - \omega_0'^2}, \qquad (5)$$

where E_0 is the amplitude of the dominant mode which is constant over the cavity length, $0 \leq z \leq L$. The coefficient η_n is determined by boundary conditions at the coupling hole; $\eta_n = 1$ if the n^{th} normal mode field at the hole has a configuration similar to that of the dominant.

Then, the hybridization of nearby modes gives a phase shift which varies along the length. A comparison between the calculated and the measured steady-state phase shifts for the AGS linac cavity is shown in Fig. 1.[7] Since the AGS linac is driven at about the center of the cavity ($z \approx L/2$), the phase shift is refered to this particular point. In the calculation, only n = 1 and n = 2 modes were taken into account; errors due to the neglected higher modes will be less than 10 %. As parameters we took:

$$\eta_1 = 0.1, \quad \eta_2 = 1,$$

$$\omega_1 - \omega_0 = 2\pi \times 33 \text{ kc},$$

$$\omega_2 - \omega_0 = 2\pi \times 125 \text{ kc, and } Q_0 = 8 \times 10^4.$$

For a transient build-up, extra power flow is necessary in order to increase the stored energy within the cavity. Correspondingly, extra phase shift due to nearby mode excitations is required. In addition, free oscilations of nearby modes are also excited, leading to beats between the nearby normal mode and the driving frequencies. Thus wiggles due to the beats appear both in the transient phase shift and the amplitude.

In general, the analysis of a transient is a complicated problem which depends upon boundary conditions at coupling holes and build-up characteristics of the generator. Fig. 2 and 3(a) show typical results of the calculation for the AGS linac by using the assumption of a well-padded generator with a step-function build-up. The calculated curves are directly compared with the measured points (maximum and minimum phase shifts) in Fig. 2[7] and the photograph of the observed build-up curve in Fig. 3(b).

4. Effects of Beam Loading in Drift Tube Cavity

4. a. Field Induced by Beam

Neglecting interactions between the beam and the generator, we can calculate the field induced by the beam separately. The sum of components of the fields from the generator and those from the beam gives the total cavity field with beam loading.

After some simplification, the field induced by the beam on the axis can be written as,

$$E_b(t) = -r_e I_0 \frac{f_0}{T_0} \frac{Q}{Q_0} e^{j\varphi_s} \left[1 - e^{-\frac{\omega_0'}{2Q}(t-t_0)}\right], \quad (6)$$

except the time variation of $e^{j\omega_0 t}$. In this formula,

- r_e : effective shunt impedance
- I_0 : beam current averaged over bunches
- φ_s : stable phase angle of beam bunches
- f_0 : form factor due to phase spread of particles in a bunch.
- T_0 : transit time factor
- Q : total Q ; $Q^{-1} = Q_0^{-1} + Q_{ext}^{-1}$
- t_0 : time when a beam comes in (beam continues to $t \to \infty$.)

The form factor, f_0, can be calculated for some simple shapes of bunches; Fig. 4 shows two examples for which a square and a half cosine like distributions are assumed. If the phase spread is less than 60°, one may assume as $f_0 = 1$.

It can be shown from the normal mode analysis that, if many bunches are distributed over the cavity length, then these bunches give very small excitations to nonsynchronous modes even to the nearest one. This corresponds to the physical arguments that, for a nonsynchronous mode, particles will travel throughout the cavity almost without being affected by the field, and that, at any moment, the fields of all of the bunches are superimposed with the proper phase relations only for a synchronous mode. Thus the field induced by the beam builds up exponentially with the rise time of the dominant mode and any wiggles do not appear (see also Fig. 5(a)).

Corresponding to the minus sign of Eq. (6), the induced field is 180° out of phase with respect to the beam bunches. The phase stable angle φ_s is usually chosen to be a few tens of degrees behind the resultant field within the cavity. Then, the real and the imaginary part of E_b give the resistive and the reactive loadings, respectively. Taking parameters,

$$r_e = 40 \text{ M}\Omega/\text{m}, \quad \varphi_s = -30°, \quad f_0 = 1,$$

$$T_0 = 0.8, \quad \text{and } Q_0 = Q_{ext} = 8 \times 10^4,$$

one obtains a maximum field decrease of about 0.18 MV/m for a 20 mA, 40 μsec beam in the AGS linac. The observed value is 0.16 MV/m and is almost constant over the cavity length (Table I).

4. b. Beam Loading Compensation

Then, we consider beam loading compensation. Unless we use widely distributed power feeds along the cavity length, it is impossible to make a perfect compensation of beam loading. The compensation can be achieved for the dominant mode. As discussed above, however, the main and compensation pulses excite nearby modes, whereas the beam gives very small excitations to those modes. This leads to the imperfection of the beam loading compensation as shown in Fig. 5(b) and Fig. 6. In Fig. 6, time variations of wiggles after compensation are magnified by taking top 10 % of the signals from the pick-up electrodes located at typical points along the length.[7]

At the existing AGS linac, the compensation pulse is added to the main pulse by increasing output of the power amplifier for the duration of the beam pulse. Since the compensation pulse has a slower build-up than the beam pulse, the analysis of the observed imperfection is a little complicated. Using the Laplace transformation method for the pulse of a finite rise time, we obtain the calculated z and time dependences of the residual effects after compensation --- in remarkably good agreements with the observations. Fig. 7 shows a comparison between the calculated and the measured amplitude of the residual uneven field along the axis. Fig. 8 gives extra phase shift along the length which is predominantly due to nearby mode excitations in the compensation field and almost independent of the presence of the beam. If, however, one takes the same value of the cavity fields for the cases with and without beams, then the extra phase shift corresponds to the extra power flow absorbed in the beam.

For an optimum compensation, both the amplitude and the extra phase shift are proportional to the beam current. Therefore, if a beam of about 100 mA is accelerated by the existing AGS linac, then the imperfectness will amount to 5 percent in the amplitude and 10 degrees in the phase shift, unless a different compensation technique is used. The field error of 5 percent also will be equivalent to a change of about 15 degrees in the synchronous phase angle, and these values will exceed tolerable errors. The time variation of wiggles during the beam pulse will cause a dynamic change of the phase bucket, which leads to appreciable losses of ions during the acceleration and a large energy spread of the output beam. In addition, the dynamic change in the longitudinal phase motion will affect the transverse motion of particles and result a dynamic variation in the emittance diagram. An example of such effects has been reported by Taylor and Dupis for the CERN-PS linac.[9] A similar result is also shown in Table I, where beam loading effects in the AGS linac are shown for typical values of currents. Even for the case without beam loading compensation, for which about 10 % field change with 20 mA loading exsists, almost the maximum capture efficiency of the linac to input currents can be achieved by means of an increase in the accelerating field. However, on account of the time variation of the field during the pulse, output beam has a large energy spread and a smaller percentage of the particles accepted in the AGS.

4. C. Possible Improvements

All of the effects discussed in the preceding paragraph are nearly proportional to the square of the distance between the driving point and the farthest point from the driving. Therefore, a shorter cavity or a system of multiple feeds has an advantage of relative immunity from beam loading. In particular, the double feeds will have the advantage of being convenient to control the phase and the amplitude independently, and, if the cavity is fed at two points each at a quarter of the total length from each end, then the nearest higher mode excited can be raised to n = 4 or the TM_{014} mode.

There will be a number of other possbilities of reducing the nearby mode excitations. Giordano has proposed to use a multistem drift tube cavity in which the mode spacing near the zero mode is a few times as great as that for the usual one or two stem cases.[10] Also, another approach will be made from considerations on the transient phenomena. The use of the transient build-up of the main pulse for beam loading compensation, such as being proposed by Carne and Batchelor,[11] will be favorable in this respect, too. Otherwise, if the beam pulse is raised slowly similar to the compensation pulse used in the AGS linac, then the amplitude of uneven field will be reduced to at least a half. The calculation shows that the AGS compensation pulse with a finite rise time of about 15 μ sec will give smaller excitations of nearby modes than the case of a step-function build-up by a factor of $2/\pi$ for n = 1 and 1/10 for n = 2. In the above experiments, such a suppression was not effective due to the fast rise of the beam pulse which results a build-up of the dominant mode different from that of the compensation.

Table I - A Measurement of Beam Loading Effects in the AGS linac

	I	II	III	IV
Compensation	No	Yes	No	Yes
Current output (mA)	21	21	10	10
Current input (mA)	60	60	—	—
Maximum field change at center Obs. (MV/m)	0.16	0.04	0.08	0.02
Calc. (MV/m)	0.18	0.03	0.09	0.015
Energy spread of output beam (half width, MeV)	0.35	0.16	0.24	0.18
Number of particles accl'd by AGS ($\times 10^{12}$ ppp)	0.62	1.08	0.42	0.57

Table II - Induced field and phase difference between the resultant field and the driving field calculated for a steady state operation of the AGS Conversion Program Linac with a 100 mA beam

Cavity Number	Et (aver) MV/m	Eb (aver) MV/m	$\Delta\varphi$ degree
1	1.7	2.5	15
2	2.3	2.9	14
3	2.5	2.5	13
4	2.45	2.1	12
5	2.40	1.9	11
6	2.35	1.7	11
7	2.30	1.5	10
8	2.25	1.4	10

4. d. Effect of Reactive Loading

Finally the reactive beam loading leads to the phase shift between the resultant cavity field and the driving field from the generator. This phase difference is given by

$$\tan \Delta\varphi = \frac{|E_b| \sin \varphi_s}{|E_t| + |E_b| \cos \varphi_s} , \qquad (7)$$

where E_t is the amplitude of the resultant field. Therefore, to obtain an optimum compensation, it is not only necessary to add an extra power flow but also to adjust the phase. If one uses a separate generator for compensation, this can be done by a phase shifter between the main and the auxiliary generators. On the other hand, if one uses one generator for two purposes, he may have to change the phase of the driving wave corresponding to beam currents. In particular, in an accelerator composed of a number of separated tanks, phases between the tanks should be adjusted for higher currents. As a numerical example, we take the new injector for the AGS Conversion Program.[12] The calculated values of E_b's and $\Delta\varphi$'s for various tanks with a 100 mA beam are listed in Table II. This predicts that, in order to keep the phase stable angle at the designed value (-25°), it will be necessary to adjust the relative phase angles between tanks over 5 degrees.

5. Effects in Multicell Cavity

The preceeding analysis has a straightforward application to a loosely coupled multi-cell cavity. In particular, the π-mode operation in a multi-cell cavity is essentially the same as the zero-mode operation used in a drift-tube cavity. We may illustrate this by using the dispersion relation with losses. With the aid of Floquet's theorem, the normal mode analysis can also derive the dispersion relation.[13, 14]

As the result, the dispersion relation for a uniform cell structure, in which we can no longer neglect wall losses, can be written

$$\omega_0^2 - \omega^2 - (1 - j)\, \frac{\omega\omega_0}{Q_0} = B(1 - \cos kL_0). \qquad (8)$$

In this expression, B depends on the cell to cell coupling and, neglecting the losses at the coupling, we may assume that B is a real number proportional to the so-called band width, $(\omega_\pi - \omega_0)$. The frequency ω is also real for a steady state. The cell length is given by L_0 and k $(= k_1 + jk_2)$ is the complex propagation constant. The dispersion curves determined by Eq. (8) are similar to those given in Fig. 9, where k_1 and k_2 are separately shown as functions of ω. From this figure, we see that, in the neighborhood of the zero- and the π-modes, the actual dispersion curves differ remarkably from those obtained for an ideal structure without losses. This is because there is no Poynting vector along the length either for the zero- and the π-normal mode field. No stop band does appear and rapidly varying curves exsist between $\omega = 0$ and the zero normal mode frequency, and between $\omega = \infty$ and the π normal mode frequency. The pure zero or π-modes can not exsist in an actual cavity; instead, apparent zero- or π-modes which have a phase shift per cell,

$$(\delta k_1 \cdot \delta k_2) L_0^2 = \frac{\omega_0^2}{Q_0 B} . \qquad (9)$$

This type of phase shift, first derived by Nagle and Knapp by using an equivalent circuit analysis,[5] is accumulated from a cell to the next leading to a square dependence on cell numbers. Since the multicell cavity has a loose cell to cell coupling compared to the drift-tube cavity, typical values of the accumulated phase shift reach some ten degrees. These values are also remarkably affected by beam loading as discussed in the preceeding paragraph, so that the π-mode uniform cell structure is extremely sensitive to beam currents.

On the other hand, Fig. 9 also shows that the least sensitive point to these perturbations is at around the middle of pass passband, or the π/2 mode. The normal mode configuration can be realized without phase shifts except a small attenuation of the field due to the losses along the length. This is the reason that the π/2 mode multicell structure has the advantage of relative immunity from effects of beam loading, tank detuning, and any other perturbations. Brookhaven explored an alternating periodic π/2 mode structure[14, 15] and Los Alamos the same type coupled by side cavities[16]. Corresponding to the double periodicity, the dispersion curve of these structures splits into two passbands and the splitted π/2 modes are essentially cut-off modes similar to the π mode. However, by means of a slight change in the zero normal-mode frequency of one of the two cell types, we can join two passbands at the π/2 mode eliminating the stopband. Even when a small splitting $\Delta\omega_{\pi/2}$ remains, we can show that the band-width parameter B in Eqs. (8) and (9) is effectively amplified by a factor of $(\omega_{\pi}-\omega_0)/\Delta\omega_{\pi/2}$ for the APS π/2 mode operation.

6. Conclusion

In conclusion, if the beam current is less than 100 mA, then the effects of beam loading in proton linacs will be moderate, and the practical design will be a compromise with some other factors. However, for a higher current, the design study will be primarily restrained by beam effects. It should also be noted that, the higher current, the more stability of the ion source and other parameters associated with the beam is required. If the beam current fluctuates about 10 % at 100 mA, then almost the same percent of the resultant cavity field will change according to the change in the induced field. Thus an automatic control system for the cavity field will be necessary for the stable beam operations.

Although the analysis discussed above is based on several simple assumptions for cavity structures, beam characteristics, and generator performances, the method will be applied to the design study of any standing-wave linacs with considerable beam loading effects.

Acknowledgement

The work reported here was done at Brookhaven National Laboratory where the author visited for the duration from May 1964 to February 1966. He would like to express his thanks to the members of the Accelerator Department, especially to Dr. Kenneth Batchelor, Dr. John P. Blewett, Mr. Salvatore Giordano, Professor Robert L. Gluckstern, Mr. John T. Kean, and Dr. George Wheeler, for their contributions through many conversations and discussions.

References

1. Among a number of reports, the reader is refered to papers by R. B. Neal, J. Appl. Phys. 29, 1019, 1958, and J. E. Leiss, Minutes of the Conference on Proton Linear Accelerators at Yale University, p. 74, 1963

2. For a more detailed review of rf structure of proton linacs, see G. W. Wheeler and S. Giordano, I.E.E.E. Trans. Nucl. Sci. NS-12, No. 3, 110, 1965.

3. P. M. Lapostolle, CERN Int. Rep. AR/Int. SG/65-9 and SG/65-12, 1965

4. T. Nishikawa, BNL Int. Rep. AADD-87, 1965. A brief report has been presented at V International Conference on High Energy Accelerators at Frascatti, 1965.

5. D. E. Nagle and E. A. Knapp, Minutes of the Conference on Proton Linear Accelerators at Yale University, p. 171, 1963 ; D. E. Nagle, Minutes of the 1964 Conference on Proton Linear Accelerators, MURA-714, p. 21, 1964. See also H. J. Hereward, CERN Int. Rep. MPS/DL, Int. 65-1, 1965.

6. J. C. Slater, Microwave Electronics, p. 66, D. Van Nostrand, New York, 1950

7. Experimental data in Figs. 1, 2, 6, 7, and 8 are quoted from the measurements by K. Batchelor and T. Werntz with their collaboration and permission. See K. Batchelor, T. Werntz and R. Chasman: Proceedings of the 1966 Linear Accelerator Conference, p. 28, and a paper to be published in BNL Int. Rep.

8. J. T. Kean, Minutes of the 1964 Conference on Proton Linear Accelerator, MURA-714, p. 398 (1964)

9. C. S. Taylor and Y. Dupis, ibid. p. 239

10. S. Giordano, Proc. of the 1966 Linear Accelerator Conference, Los Alamos, p. 88.

11. A. Carne and K. Batchelar, RHEL Int. Rep. NIRL/R/55, 1964.

12. Alternating-Gradient Synchrotron Conversion Program, Scope of Phase 1, BNL 9500, Brookhaven National Laboratory, 1965.

13. T. Nishikawa, I.E.E.E. Trans. Nucl. Sci. NS-12, No. 3, 630, 1965.

14. T. Nishikawa, S. Giordano, and D. Carter, Rev. Sci. Instr. 37, 652, 1966, See also J. P. Blewett, BNL Int. Rep. AADD-65, 1965.

15. S. Giordano, ibid. p. 213

16. E. A. Knapp, Minutes of the 1964 Conference on Proton Linear Accelerators, MURA-714, p. 31, 1964 ; B. C. Knapp, E. A. Knapp, G. J. Lucas, and J. M. Potter, I.E.E.E. Trans. Nucl. Sci. NS-12, No. 3, 159

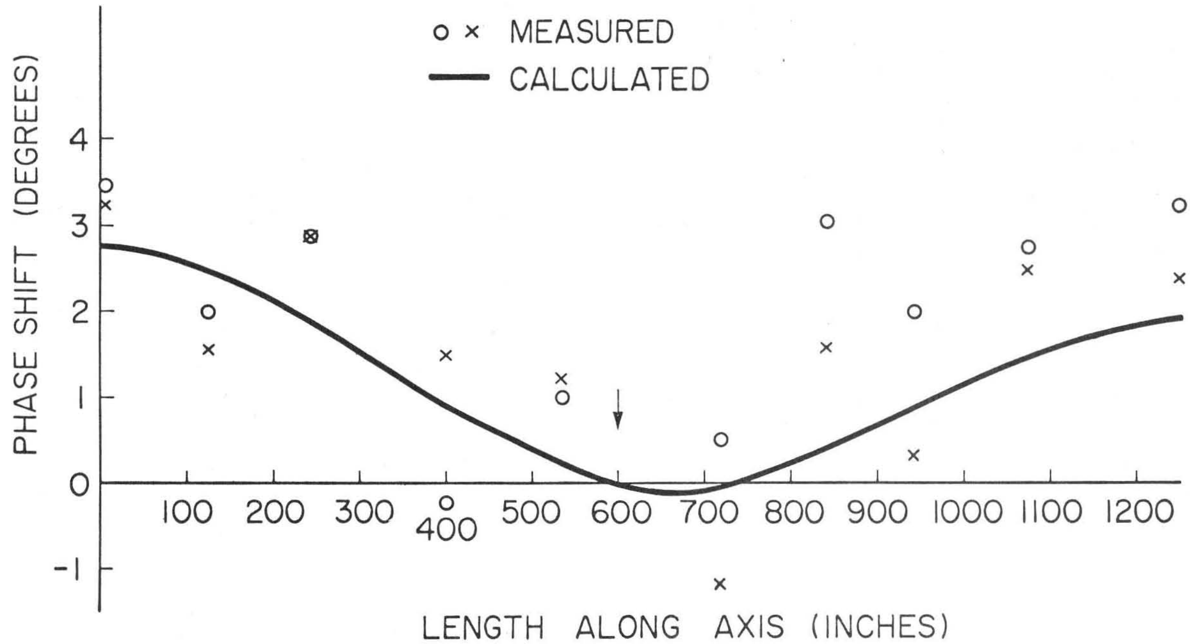

Fig. 1. Steady state phase shift along AGS linac cavity referred to the driving point (near the center of cavity).

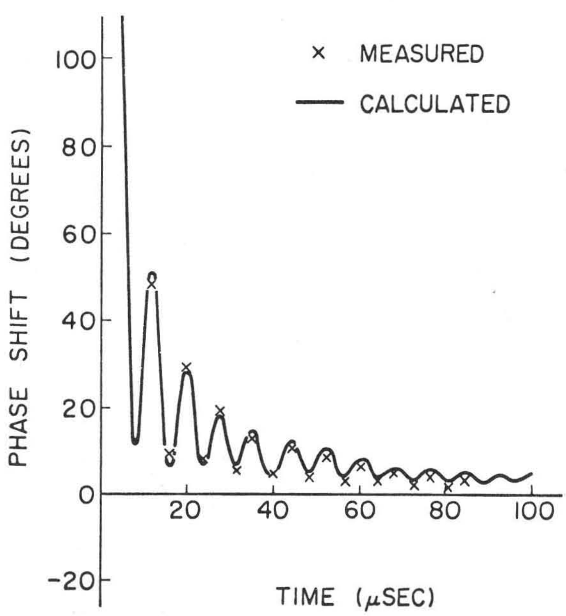

Fig. 2. Transient phase shift between the center and the low energy end of AGS linac cavity.

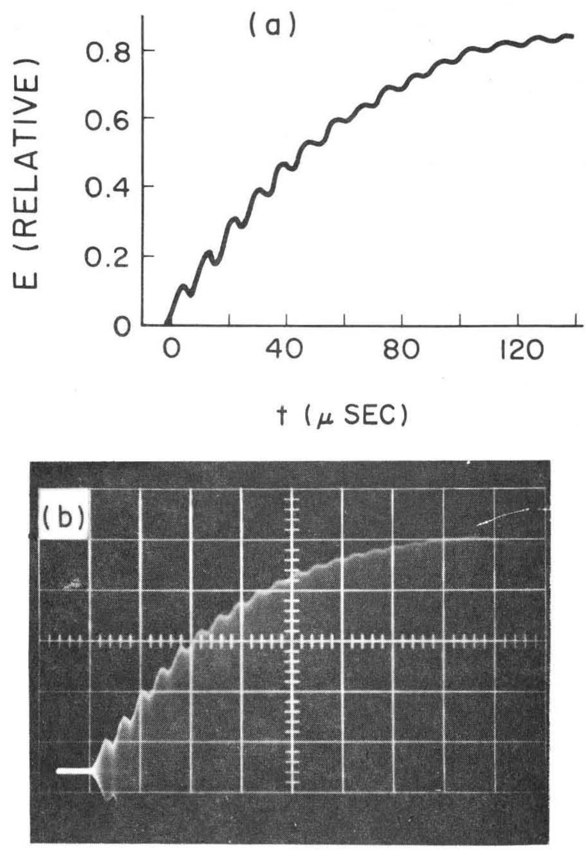

Fig. 3. Transient build-up of the field near the center of AGS linac cavity. (a) Calculated from the normal mode analysis; (b) Observed by a pick-up electrode (20 μsec/div).

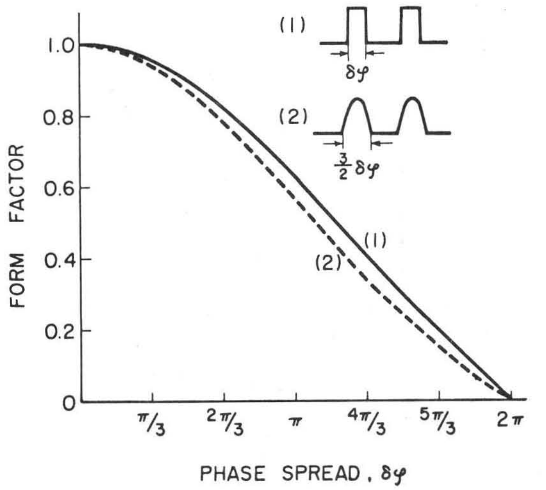

Fig. 4. Form factors for typical shapes of beam bunches. (1) Square wave type with the width of δφ. (2) Half cosine wave type with the total width of 3/2 (δφ).

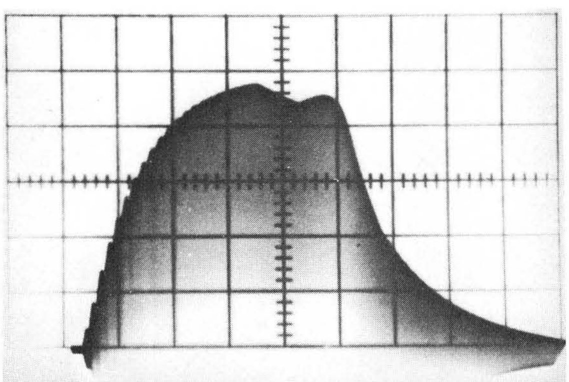

Without compensation.

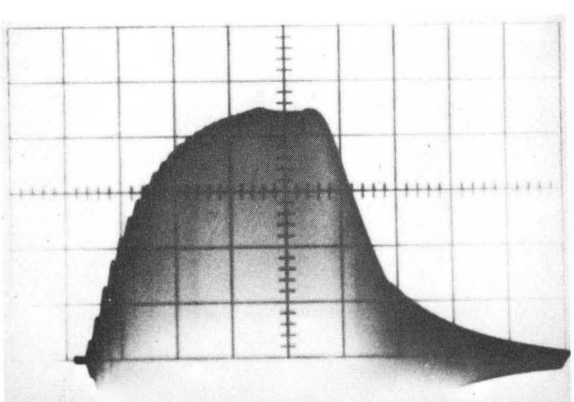

With compensation (Compensation is almost perfect near the low energy end of the cavity.)

Fig. 5. Effect of beam loading in the RF-field pattern near the center of AGS linac cavity (50 μsec/div; beam current of 20 mA, 40 μsec).

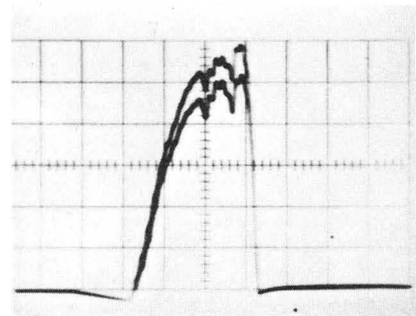

$z \approx 0$

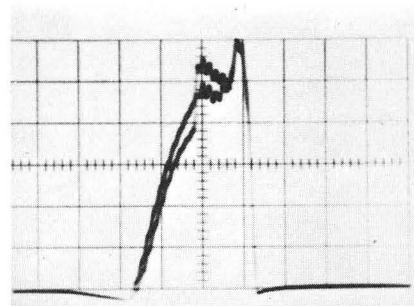

$z \approx L/2$

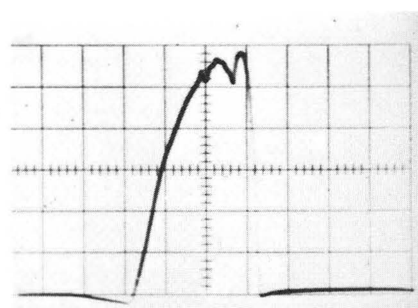

$z \approx L/4$

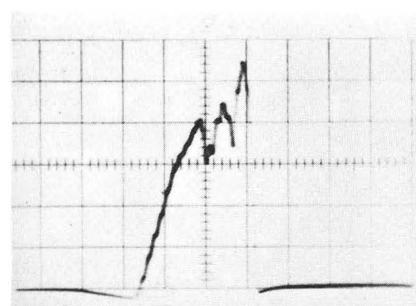

$z \approx L$

Fig. 6. Magnified effect of incompleteness of beam loading compensation in AGS linac cavity showing wiggles due to nearby mode excitations by compensation pulse (50 μsec/div; beam current of 32 mA with pulse length of 40 μsec).

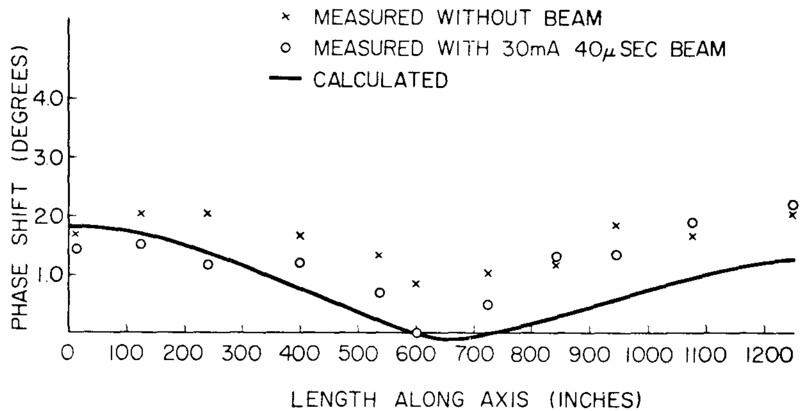

Fig. 7. Amplitude of uneven field in AGS linac cavity after an optimum compensation. Beam: 30 mA with 40 μsec square pulse. Compensation: a slowly build-up pulse with rise time of about 15 μsec.

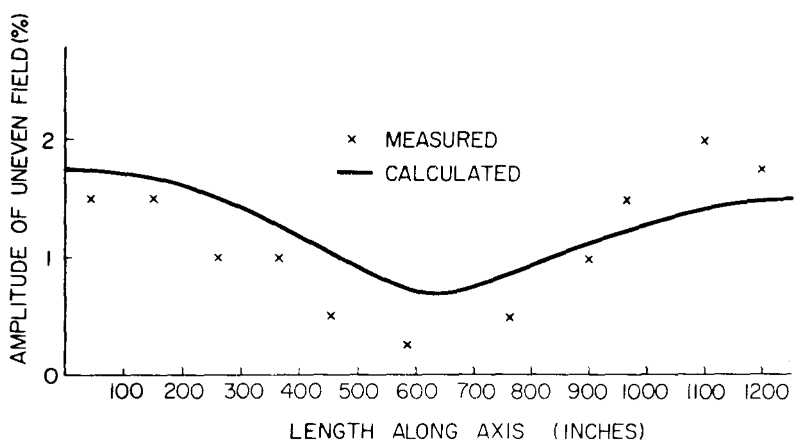

Fig. 8. Extra phase shift due to the compensation pulse applied to AGS linac cavity. (Maximum values for time variations. The beam is the same as in Fig. 7, while the compensation is about 60% compared to the optimum value.)

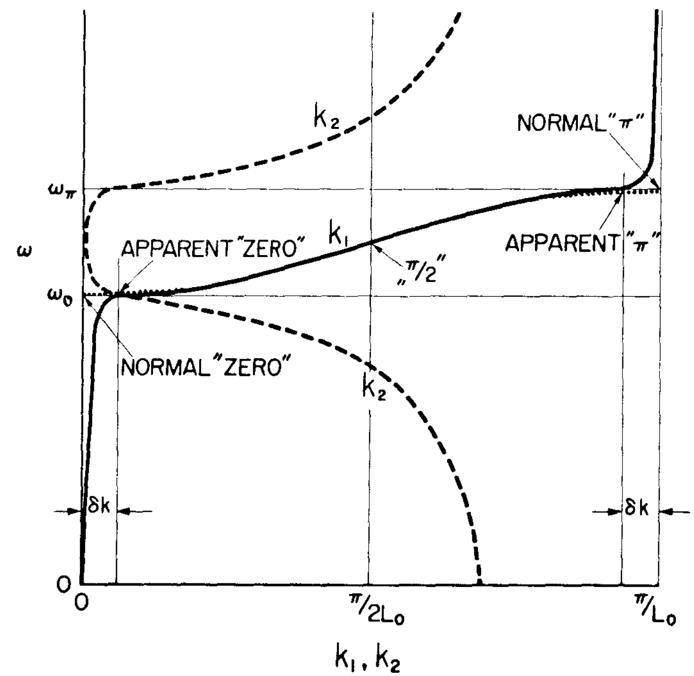

Fig. 9. Dispersion curves for uniform multicell structures with losses. The dotted cosine-like curve shows the case without losses. (k_1, k_2: real and imaginary part of propagation constant, k. The magnitude of δk_i is approximately given by $|\delta k| \approx 1/L_0(\omega^2/Q_0 B)^{1/2}$.)